Human-Centered Functional Task Design for Robotic Upper-Limb Rehabilitation

Anna Bucchieri[1,3], Federico Tessari[2], Stefano Buccelli[1], Giacinto Barresi[1], Elena De Momi[3], Matteo Laffranchi[1], Lorenzo De Michieli[1]

Abstract— Robotic rehabilitation has demonstrated slight positive effects compared to traditional care, but there is still a lack of targeted high-level control strategies in the current state-of-the-art for minimizing pathological motor behaviors. In this study, we analyzed upper-limb motion capture data from healthy subjects performing a pick-and-place task to identify task-specific variability in postural patterns. The results revealed consistent behaviors among subjects, presenting an opportunity to develop a novel extraction method for variable volume references based solely on observations from healthy individuals. These human-centered references were tested on a simulated 4 degrees-of-freedom upper-limb exoskeleton, showing its compliant adaptation to the path considering the variance in healthy subjects' motor behavior.

Index Terms— Upper-Limb, Exoskeleton, Path, Multi-Body, Motor-Control

I. INTRODUCTION

Upper-Limb impairments can be the result of different causes such as musculoskeletal disorders or neurological accidents. Even though the two causes lead to different form of impairments and rehabilitative journeys, both the affected patients suffer from the loss of ability in performing activities of daily living (ADLs) [1]–[3]. Robotic platforms represent a powerful tool to promote motor strengthening and neuro-plasticity, by providing intensive and repetitive exercises [1]–[7]. However, some studies reported only minor improvements in robotic-assisted therapy with respect to usual care [6] [8], especially in terms of motor functionality. Brewer et al. highlight how thanks to robotic systems it will be possible to standardize movements and rigorously test them [7], but we still miss proper scales of measurements to correctly differentiate genuine upper-limb motor recovery from functional one due to compensation strategies [9]–[12]. From studies on upper-limb motor behaviour of healthy subjects it is established that, despite the characteristic redundancy of the arm, the human motor control strategy for reaching a point in the space is reproducible, and show similar and repetitive characteristics in terms of hand paths and velocity profiles [14]–[17–27]. On the contrary, such patterns seem to be initially altered in post-stroke patients, but after a rehabilitative period kinematic profiles tend to converge

toward the physiological one investigated on healthy subjects [18]. This important finding opens the possibility to exploit kinematic measurements for the evaluation of ADLs recovery [7] [18]. During complex movements like pick-and-place tasks commonly used in Occupational Therapy, several phases are involved. After picking up the object, the hand accelerates towards the target, followed by a corrective control strategy to refine object placement. These phases result in varying levels of variability in healthy postural patterns. Previous studies have proposed path-based control strategies with fixed-radius haptic tunnels, utilizing specific geometrical patterns [19]–[21]. However, such approaches may be limiting when applied to ADL. The correction and assistance provided by the robot should be adaptable to the characteristics of each task. Currently, there is a lack of optimal robotic strategies that specifically address compensating for kinematic discrepancies in ADLs tasks for impaired individuals, while considering the variability seen in the able-bodied population [7].

In this study we present a novel approach in which, starting from the observation of 14 healthy subjects while performing a pick-and-place task, it is possible to create scalable volume-specific references for the control of a simulated 4 deegrees-of-freedom (DOF) exoskeleton, a new prototype developed by Istituto Italiano di Tecnologia [22]. Partiuclarly, we simulated a force-field algorithm based on the generated volumes, to provide both a correction normal to the desired trajectory and a corrective-assistance toward the completion of the task, tailored on healthy movements variability while performing the specific case study.

II. MATERIALS AND METHODS

A. Participants

The Vicon Nexus 2.12.1 motion capture system (MoCap) was used to acquire kinematic data from subjects (Fig.1A). The subjects wore twelve infra-red reflective markers on their right arm, useful to create a biomechanical model of the right upper-limb (Fig.1B). This work was conducted in accordance with Protocol "IIT_REHAB_HT01 N. Registro CER Liguria: 363/2022 - DB id 12494". For the acquisition of human-based references we recruited 14 right-handed healthy subjects, 7 male and 7 females between 25 and 30 years-old. People from the 23rd female to 99th male height percentiles were selected in order to investigate the performance of movements in a highly variable subjects' population.
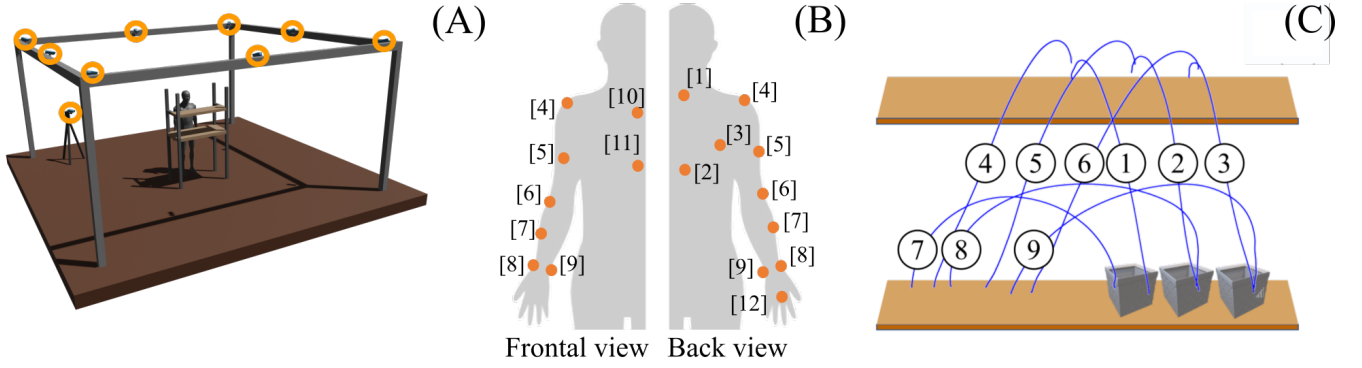
Fig. 1: Experimental set-up. (A) Environment where MoCap acquisitions were performed. Highlighted in orange 9 Neuxs Vicon infrared cameras used. At the centre of the room a representation of the library used to perform the pick-and-place task. (B) Positioning of IR-reflective markers on subjects. [1]C7, [2]T10, [3]Scapula, [4]Shoulder, [5]Arm, [6]Elbow, [7]Forearm, [8]Outer Wrist, [9]Inner Wrist, [10] Collar bone, [11]Sternum, [12]Knuckle (C) Visualization of the task: movements from table to shelf (MOV1, MOV2, MOV3), from shelf to table (MOV4, MOV5, MOV6), and from table to table (MOV7, MOV8, MOV9).

B. Experimental Protocol

Subjects performed a pick-and-place task involving three plastic boxes (10x8x9.5 cm, 0.2 kg each) on a movable structure resembling a table and a shelf (Fig.1A). The shelf height was adjusted to shoulder height, with the table positioned 40 cm below the shelf for all subjects. The experimental session began with an explanation of the study's objective. Subjects were instructed to pick boxes from a designated location on the library and place them in a specific target. The task was repeated three times, and participants were encouraged to perform the movements in a relaxed and comfortable manner, without time and path constraints. Nine movements were tested (Fig.1C):

- From table to shelf (MOV1, MOV2, and MOV3);
- From shelf to the table (MOV4, MOV5, and MOV6);
- From the late position back to their starting position on table (MOV7, MOV8, and MOV9).

C. Data analysis

We focused solely on the acquired knuckle trajectories (Fig.1B), which are considered a reliable representation of the arm end-effector path. Data analysis was conducted using MATLAB R2021b. To determine if the duration of all trials followed a normal distribution, a Shapiro-Wilk test was performed. Results for each movement showed a slight positive skew, therefore data timing distribution is not normal for all movements. However, this outcome could be attributed to the small dataset size. Since the goal of the study is to explore the average behaviour of healthy subjects, we decided to include in our calculations only the data points with duration falling inside one standard deviation from the mean movement time ($\mu \pm 1\sigma$). Finally, the data were averaged across repetitions and subjects, resulting in 9 mean trajectories representing the 9 movements.

D. Reference volumes and Vector-Field generation

In this paper we will address the resultant trajectory for each movement averaged on repetitions and subjects as Γ. For each task we calculated the standard deviation σ in x,

y, and z across trials. These data were exploited to create a volumetric shape centred in Γ and variable radius R (Fig.2C), calculated as the average between σ^x, σ^y, and σ^z for each point of Γ:

$$C_\Gamma^R(i_\Gamma) \in (\Pi \perp \vec{\Gamma}(i_\Gamma+1) - \vec{\Gamma}(i_\Gamma), \text{ for } i_\Gamma \in [0, size(\Gamma)] \quad (1)$$

where $C_\Gamma^R(i_\Gamma)$ represents a circular section of the tunnel.

Once the volumetric shapes were optimized, we implemented a compliant control strategy. Given the position of the exoskeleton end-effector $\vec{P}_{EE}$ in the space, the control calculates the corrective ($\vec{F}_C$) and corrective-assistive ($\vec{F}_A$) forces needed to minimize the error between the actual position $\vec{P}_{EE}$ and the desired one belonging to Γ:

$$\vec{F}_{control} = \begin{cases} \vec{F}_C \text{ if } ||\vec{P}_{EE} - \vec{\Gamma}(i)|| - R(i) > 0 \\ \\ \vec{F}_A \text{ otherwise} \end{cases} \quad (2)$$

where $\vec{\Gamma}(i)$ the closest point of the trajectory Γ to the end-effector position $\vec{P}_{EE}$ such as $min||\vec{P}_{EE} - \vec{\Gamma}(i)||$, calculated through a k-nearest-neighbors algorithm. In Fig.2A and B we reported a schematic on how the two components were computed. In particular, the corrective component is perpendicular to $(\vec{\Gamma}(i) - \vec{\Gamma}(i-1))$:

$$\vec{F}_C = (K_c \cdot \Delta d + \beta_c \cdot \Delta \dot{d})\vec{n} \quad (3)$$

where Δd is the distance $||\vec{P}_{proj} - \vec{P}_{EE}|| - R(i)$, $\vec{n}$ defines the normalized direction $\frac{\vec{P}_{proj} - \vec{P}_{EE}}{\Delta d}$, $\vec{P}_{proj}$ is the projection of the $\vec{P}_{EE}$ in the line defined by $(\vec{\Gamma}(i) - \vec{\Gamma}(i-1)$, and (Fig.2A). K_c and β_c are the constant stiffness and damping coefficients of an impedance filter, which were set to $K_c = 400$ N/m and $\beta_c = 40$ Nm/s on the multi-body simulation.

On the other hand, we defined an assistive and corrective force $\vec{F}_A$ toward $\vec{\Gamma}(i+1)$ (Fig.2B) and parallel to $(\vec{\Gamma}(i+1) - \vec{P}_{EE})$.

$$\vec{F}_A = (K_a \cdot \Delta d + \beta_a \cdot \Delta \dot{d})\vec{m} \quad (4)$$

where Δd is the distance $||\vec{\Gamma}(i+1) - \vec{P}_{EE}||$, and $\vec{m}$ is the normalized vector defining the direction $\vec{\Gamma}(i+1) - \vec{P}_{EE}$.
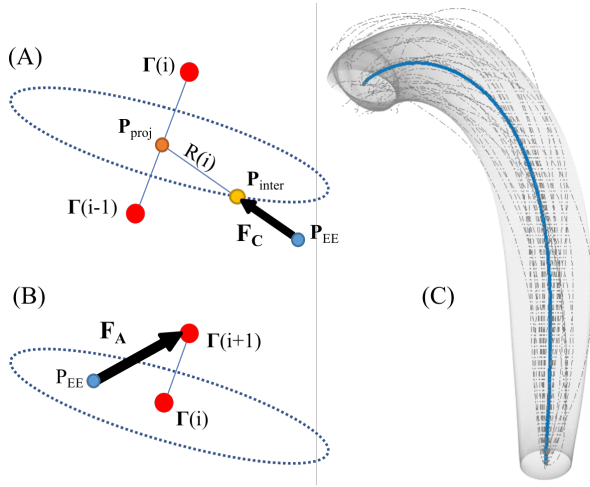
Fig. 2: Visual representation of the proposed Vector-Field algorithm and reference volume generation. (A) When the actual position of the end-effector ($\vec{P}_{EE}$) is outside of the reference volume, a force perpendicular to the line connecting the closest point of the trajectory ($\Gamma(i)$) to the previous one ($\Gamma(i-1)$) is computed. The module of this force is a function of the distance of the end-effector to the reference volume wall ($\vec{P}_{inter} - \vec{P}_{EE}$) and the radius $R(i)$. (B) When $\vec{P}_{EE}$ is inside the reference volume, both a corrective and assistive force is provided toward the next point of the trajectory $\Gamma(i+1)$, which will help the user follow the optimal path without risking to get stuck inside the volume. (C) Reference volume of variable radius around the optimal trajectory Γ (in blue), generated by averaging all trials (in scattered gray) while performing MOV1 (table to shelf)
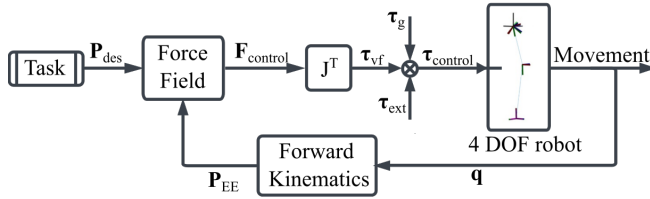

Fig. 3: Torque control with a closed-loop in joint positions ($\vec{q}$). The total torque control is the result of different contributions such as the vector-field one $\vec{\tau}_{vf}$, the gravity compensation $\vec{\tau}_g$ and the external disturbances $\vec{\tau}_{ext}$. $\vec{P}_{des}$ represents the closest point of the optimal trajectory to the end-effector $\vec{P}_{EE}$.

K_a and β_a are the stiffness and damping coefficients of an impedance filter, which were set to $K_a = 400$ N/m and $\beta_a = 40$ Nm/s on the multi-body simulation. When $\vec{P}_{EE}$ is close to $\vec{\Gamma}(i)$, the direction $\vec{m}$ becomes normal to the reference $C_\Gamma^R(i)$ (Eq.1) and $\vec{F}_A$ becomes only an assistive force toward $\vec{\Gamma}(i+1)$ (Fig.2B).

E. Multi-Body simulation and control strategy

Simscape MATLAB R2021b was employed to create the model of a novel upper-limb exoskeleton developed by Istituto Italiano di Tecnologia, based on a previous version [22]. With respect to industrial secrecy, its mechatronics cannot be disclosed in this manuscript. The model solely presents the glenohumeral and elbow revolute joints (4 DoFs). We decided to test the control exclusively on the MOV1 acquired (Fig.1C). As a consequence, wrist displacements can be omitted since this physiological joint does not come into play while performing MOV1 in this specific set-up (more details in Section III). Each link of the robot was provided with

mass and inertial characteristics as in the prototype. Then, we implemented the force-field based control strategy described in the previous paragraph. The proposed control strategy is a torque control with a closed-loop in Cartesian position (Fig.3). Once either the correction (Eq.3) or corrective-assistance (Eq.4) is computed at a high-level, the resultant force $\vec{F}_{control}$ (Eq.2) is multiplied by the transpose of the Jacobian to obtain the joint torques $\vec{\tau}_{vf}$ to be provided to the exoskeleton.

$$\vec{\tau}_{vf} = J^T \vec{F}_{control}$$

The robot dynamic model is described as

$$M(\theta)\ddot{\theta} + C(\theta, \dot{\theta})\dot{\theta} + G(\theta) = \vec{\tau}_{control} + \vec{\tau}_{ext}$$

where $M(\theta)$ is the joint-space mass matrix, $C(\theta, \dot{\theta})$ is the Coriolis term, and $G(\theta)$ represents the gravity torques and forces required for all joints to maintain their positions. We neglected the inertial components and implemented a gravity compensation so that the system would not be affected by its own weight. The total $\tau_{control}$ input to the robot is

$$\vec{\tau}_{control} = \vec{\tau}_{vf} + \vec{\tau}_{ext}$$

The joint positions of the simulated robot are then measured and the end-effector position $\vec{P}_{EE}$ is derived through forward kinematics. To test the controller we applied an external disturbance $\vec{F}_{ext} = \vec{F}_x + \vec{F}_y$ as a squared wave of amplitude $85N$, period $10s$, and width 5% of period. This was done to validate the adaptability of the proposed controller to the variable path proposed.

III. RESULTS

A. Kinematic measurements from healthy subjects

From the considerations on the duration of trials we identified 108 curves out of 378 movement duration fell inside the ($\mu \pm 1\sigma$) condition (28.6%). The average time and standard deviation across trials for each task is reported in Table I. The following considerations solely concern the hand movements from when the object is already picked to when it is placed. The average wrist displacements in terms of flex-extensions and prono-supinations show average standard deviation of $4.5°$ and $4.8°$ respectively. Thus, hand displacements for the three sets of tasks (MOV1-MOV3, MOV4-MOV6, MOV7-MOV9) show negligible influence from wrist movements. In Fig.4A (displacement P of the hand calculated as P = $\sqrt{x^2 + y^2 + z^2}$) MOV2 and MOV3 present higher variability close to the placing phase. This is also observable in Table I where the maximum standard deviation across trials is at the edge of the path. On the contrary, MOV4-MOV6 and MOV7-MOV9 present hand paths less spread, with maximum standard deviation reached in the first half of the path (Table I). In Fig.4B the velocity profiles are reported (V = $\sqrt{V_x^2 + V_y^2 + V_z^2}$). The three sets of movements for each task present qualitatively comparable shapes. For all of the three sets, it is noticeable how the velocity profile of the first movement (MOV1, MOV4, and MOV7) is slightly different from the following two. This is reported in Table I where the fraction of path at which

the maximum velocity is reached across trials decreases across tasks. Two-way t-test performed on $\%path_{V max}$ shows a statistically significance difference between MOV1 versus MOV2-MOV3, MOV7 versus MOV8-MOV9, and no difference between MOV4 versus MOV5-MOV6. We also computed the average maximum velocity for each set of movements and we found comparable results both intra-tasks (sets MOV1-MOV3, MOV4-MOV6, MOV7-MOV9, Table I) and inter-tasks (in MOV1-MOV9). Lastly, for each movement we investigated whether the proposed tunneling shapes represent most of the trials. To do so, for each trial we computed the percentage of data points included by the volume. Then, we averaged the result on repetitions and subjects. For all of the movements we obtained that at least 78% of trial data fall inside the volumes, and the average inclusion across movements is 85.4% (Fig.2C). This is in line with the gaussian distribution hypothesis on the trajectories dataset.

B. Force-Field control strategy

When a perturbation $\vec{F}_{ext}$ is first applied to the end-effector (Fig.5C) and this is still inside the reference volume, the control force $\vec{F}_{control}$ will be given only by the corrective-assistance $\vec{F}_A$ (blue line in Fig.5A and B). Then, when the hand moves outside the tunnel, the corrective $\vec{F}_C$ (red line in Fig.5A and B) comes into play and $\vec{F}_A$ drops to zero, and vice versa when the end-effector gets back into the tunnel. Equivalent force perturbations were applied with period of $10s$ along the trajectory path: (1) at 5% of the path, where the radius of the volume is 2.3 cm, (2) at 40%, where the radius is 5.1 cm, (3) at 47%, where the radius is 4.8 cm, (4) at 49.7%, where the radius is 4.6 cm, and (5) at 52% where the radius is 4.3 cm. In condition (1) we observed - see Fig.5A - that the smaller radius immediately guarantees the switch between assistive-corrective behaviour and fully corrective, while when the radius of the reference volume grows - see case (2) toward case (5) - the duration of application of assistive-corrective action continues for longer periods of time.

IV. DISCUSSION

In this study, we examined the upper-limb motor behavior of healthy subjects during a pick-and-place task to identify specific geometric and kinematic characteristics of these movements. The composite hand displacement across trials for MOV1-MOV9 clearly exhibits a curved trend rather than a straight line (Fig.4A). This suggests that, in a pick-and-place task, subjects tend to follow a curving trajectory when not explicitly instructed to move in a straight line. The timing of movements is also consistent across trials for each movement, despite the absence of time constraints for the subjects. Notably, MOV1-MOV3 and MOV7-MOV9 show higher variation (standard deviation) along a larger portion of the path compared to when maximum velocity is reached (Table I). This indicates that in these movements, subjects initially prioritize acceleration towards the target, resulting in diverse motor behaviors, and subsequently refine
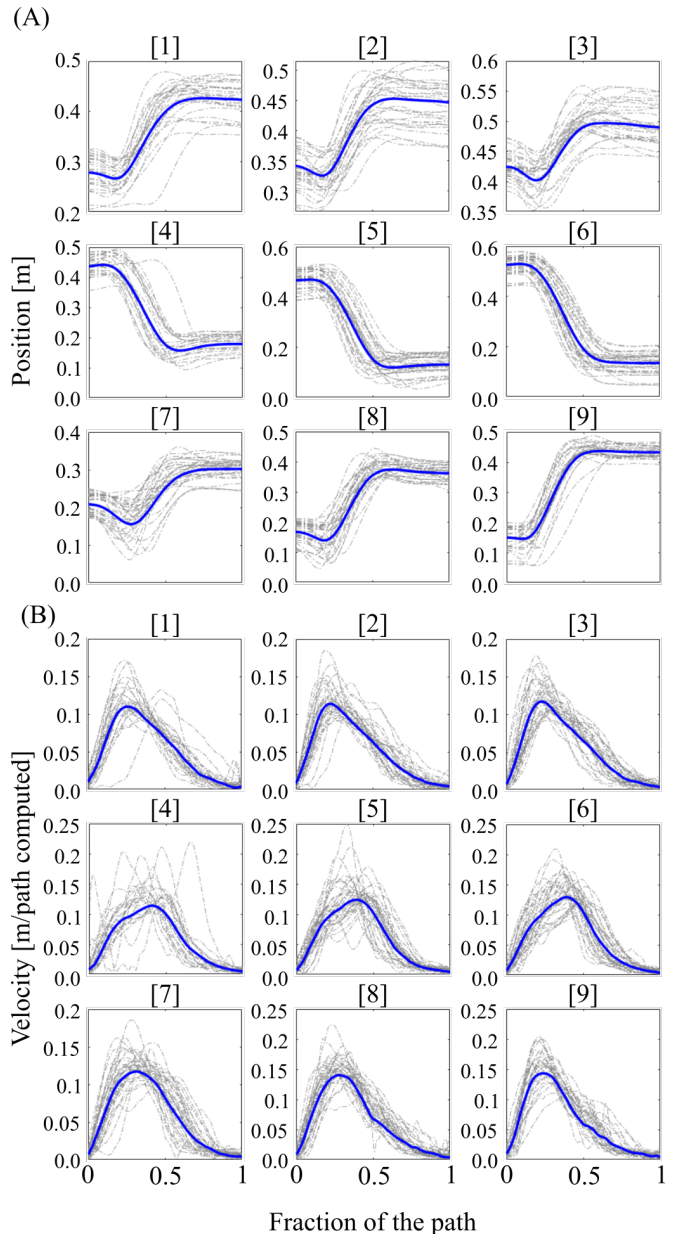

Fig. 4: (A) Representation of hand positions across trials (in grey) and the average between them (in blue) with respect to the fraction of the path. (B) Representation of hand velocities across trials (in grey) and the average between them (in blue) with respect to the fraction of the path, expressed as m/[path completed]. [1] is relative to MOV1, [2] MOV2, [3] MOV3, [4] MOV4, [5] MOV5, [6] MOV6, [7] MOV7, [8] MOV8, [9] MOV9

the movement to place the object. The same pattern is not observed in MOV4 and MOV5, where maximum variation is reached slightly before maximum speed. This suggests that, for tasks in favour of gravity, there is a tendency to initiate the movement slowly, leading to the aforementioned variability, and then accelerate towards the target. This is in line with extensive literature studies on the Fitt's Law about speed-accuracy trade-off [23]–[25]. The composite displacement of the hand seem to present smooth outlines in accordance with minimum-jerk theories, extensively studied in literature [26]–[29]. Moving on to velocity profiles, there

TABLE I: Results on timing across trials, maximum variation in path, maximum velocity $[m/\%path]$, and two-way t-test (level of significance 0.05) between $\%path_{V_{max}}$ of first movement of each set and the following two.

|	Movements	$Time \pm \sigma_{time}$ [s]	σ_{max} [cm]	% path σ_{max}	$V_{max} \pm \sigma_{V_{max}}$	$\%path_{V_{max}} \pm \sigma_{\%path_V}$	$p-value$
			Maximum σ and velocity for each movement				
	MOV1	1.76 ± 0.31	5	43.2%	1.23 ± 0.2	27.5 ± 7.65 %	-
Set1	MOV2	1.73 ± 0.44	3.8	91.2%	1.25 ± 0.21	$23.9 \pm 5.5\%$	< 0.05
	MOV3	1.53 ± 0.28	3.15	98.8%	1.28 ± 0.22	$24.3 \pm 5.2\%$	< 0.05
	MOV4	1.68 ± 0.25	7.35	40%	1.43 ± 0.32	$41.4 \pm 9.6\%$	$-$
Set2	MOV5	1.88 ± 0.45	5.38	38.3%	1.47 ± 0.3	$39.8 \pm 8.5\%$	> 0.05
	MOV6	1.71 ± 0.33	6.33	43%	1.47 ± 0.24	$40.4 \pm 7\%$	> 0.05
	MOV7	1.85 ± 0.29	4.48	42.6%	1.32 ± 0.18	$32.5 \pm 9\%$	-
Set3	MOV8	1.87 ± 0.4	4.47	24.4%	1.57 ± 0.22	$27.32 \pm 5.7\%$	< 0.05
	MOV9	1.90 ± 0.42	5.3	28.9%	1.59 ± 0.26	$24.6 \pm 6\%$	< 0.05
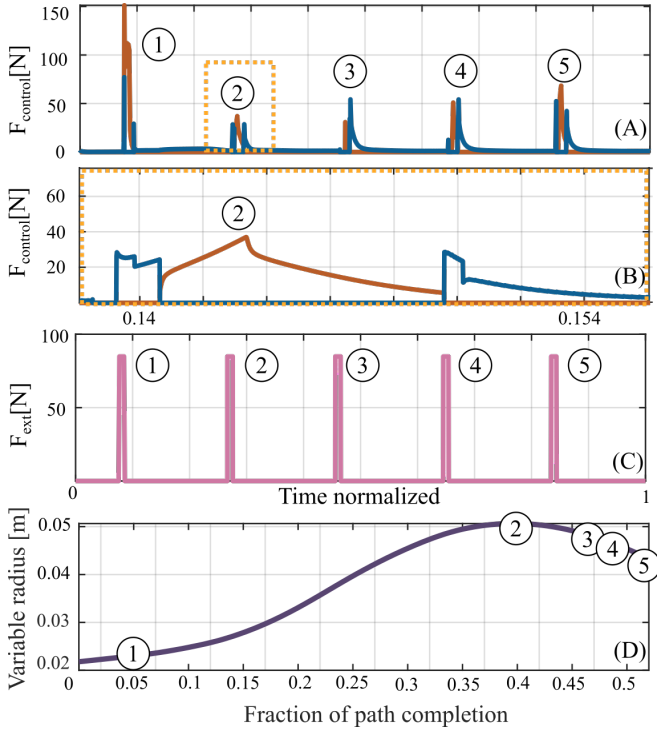
Fig. 5: (A) Contribution of the corrective forces (in red) and the corrective-assistive ones (in blue) following perturbations. (B) Closeup of the control torque. (C) External perturbations applied. (D) Variation of the radius of the created references according to the fraction of path. Circled numbers indicate at which fraction of path and radius magnitude the external forces were applied.

are noticeable patterns across movements. MOV1-MOV3 and MOV7-MOV9 exhibit a steep rising slope in the first half of the curve, followed by a smoother profile. A slight change in slope can be observed near the placing phase. On the other hand, MOV4-MOV6 show the opposite tendency, with a flatter velocity profile in the first half of the curve and a steeper one in the second half. Similarly, a slight change in slope is observed near the placing phase (Table I). These differences can be attributed to the nature of the movements: MOV1-MOV3 and MOV7-MOV9 are performed against gravity, while the others are propelled by gravity, resulting in varying slope changes. In all cases except MOV7, the curves exhibit two small bumps, which align with Abend et al.'s study on velocity profiles during curvy paths [15].

Another interesting observation relates to the velocity patterns of MOV1, MOV4, and MOV7 across trials (Fig.4B). The gray lines appear more scattered and unrelated compared to their consecutive movements (MOV2-MOV3, MOV5-MOV6, MOV8-MOV9). This may be attributed to motor learning effects, where the second and third tasks within each set show less variability; moreover, the first movement of each set appear to be influenced be the influenced by the previously adopted motor control strategy.

These initial findings demonstrate consistent and repetitive kinematic behaviors, suggesting their potential use as recovery metrics for task-specific functional rehabilitation.

Based on these results, it is essential to develop a robotic control strategy specifically focused on minimizing pathological postures. The proposed reference tunnels, centered around the mean trajectory with variable standard deviation, accurately represent the average behavior of healthy individuals performing a pick-and-place task under different conditions. The tunnels have an average maximum diameter of 9 cm [30], smaller than the average size of a human hand. However, in rehabilitation settings, these references may overly constrain movements and cause discomfort. Therefore, therapists should have the flexibility to scale the tunnels based on the user's level of impairment, progressively reducing the constraint as the user recovers. For impaired subjects, a scale factor of 3 (maximum diameter of 27 cm, nearly twice the average hand size) may be appropriate to perform the task.

Additionally, the proposed compliant control strategy demonstrated in simulations how the system can provide end-effector corrections based on the variability of the reference tunnels. The greater the radius of the tunnel, the more freedom of movement is given to the patient. The level of compliance can be adjusted by therapists through stiffness and damping coefficients in the impedance control. However, these parameters were chosen empirically in the current simulation and require further investigation.

Multi-body simulations offer a strategic and cost-effective approach to improve robotic control without compromising patient safety. Future studies are needed to determine whether following such paths in task-space translates to physiological coordination in joint-space.

Overall, these findings highlight the importance of tailored robotic control strategies and the potential of multi-body simulations in advancing rehabilitation practices.While our work has limitations in generalizing the proposed acquisi-

tions to different ADLs, the study showed how even without specific instructions or robotic constraints (e.g., MIT-Manus [5]), the kinematic behavior among healthy subjects remains comparable. Thus, the proposed setup can serve as a novel assessment tool for evaluating ADL recovery, involving object manipulation and mobilization in 3D space.

V. CONCLUSION

Recovering the skills necessary for performing ADLs poses a significant challenge for individuals with upper-limb impairments. Integrating robotic rehabilitation with a proper understanding of motor behaviors in able-bodied individuals allows for targeted assistance in regaining initial motor functions. In this study, we conducted a MoCap analysis involving 14 healthy subjects performing a pick-and-place task. From this analysis, we derived task-specific volumetric references that reflect the variability observed during their dynamic movements. Subsequently, we tested a time-independent control approach on a simulated 4 DOF upper-limb exoskeleton. Results demonstrate effective correction and assistance of end-effector movements on the extrapolated human-centered volumes. In future research, we aim to evaluate the efficacy of the proposed approach in upper-limb robotic rehabilitation by implementing the control strategy on the physical exoskeleton.

REFERENCES

[1] T. Proietti, V. Crocher, A. RobyBrami, and N. Jarrasse, "Upper-limb robotic exoskeletons for neurorehabilitation: a review on control strategies," IEEE reviews in biomedical engineering, vol. 9, pp. 4–14, 2016.

[2] H. Feys, W. De Weerdt, G. Verbeke, G. C. Steck, C. Capiau, C. Kiekens, E. Dejaeger, G. Van Hoydonck, G. Vermeersch, and P. Cras, "Early and repetitive stimulation of the arm can substantially improve the long-term outcome after stroke: a 5-year follow-up study of a randomized trial," Stroke, vol. 35, no. 4, pp. 924–929, 2004.

[3] N. Nordin, S. Q. Xie, and B. Wünsche, "Assessment of movement quality in robot-assisted upper limb rehabilitation after stroke: a review," Journal of neuroengineering and rehabilitation, vol. 11, no. 1, pp. 1–23, 2014.

[4] E. Martinez-Martin and M. Cazorla, "Rehabilitation technology: assistance from hospital to home," Computational Intelligence and Neuroscience, vol. 2019, 2019.

[5] N. Hogan, H. I. Krebs, J. Charnnarong, P. Srikrishna, and A. Sharon, "Mit-manus: a workstation for manual therapy and training. i," in [1992] Proceedings IEEE International Workshop on Robot and Human Communication, pp. 161–165, IEEE, 1992.

[6] A. C. Lo, P. D. Guarino, L. G. Richards, J. K. Haselkorn, G. F. Wittenberg, D. G. Federman, R. J. Ringer, T. H. Wagner, H. I. Krebs, B. T. Volpe, et al., "Robot-assisted therapy for long-term upperlimb impairment after stroke," New England Journal of Medicine, vol. 362, no. 19, pp. 1772–1783, 2010.

[7] B. R. Brewer, S. K. McDowell, and L. C. Worthen-Chaudhari, "Post-stroke upper extremity rehabilitation: a review of robotic systems and clinical results," Topics in stroke rehabilitation, vol. 14, no. 6, pp. 22-44, 2007.

[8] V. Klamroth-Marganska, J. Blanco, K. Campen, A. Curt, V. Dietz, T. Ettlin, M. Felder, B. Fellinghauer, M. Guidali, A. Kollmar, et al., "Three-dimensional, task-specific robot therapy of the arm after stroke: a multicentre, parallel-group randomised trial," The Lancet Neurology, vol. 13, no. 2, pp. 159–166, 2014.

[9] G. Kwakkel, B. J. Kollen, and H. I. Krebs, "Effects of robot-assisted therapy on upper limb recovery after stroke: a systematic review," Neurorehabilitation and neural repair, vol. 22, no. 2, pp. 111–121, 2008.

[10] J. Mehrholz, A. Hädrich, T. Platz, J. Kugler, and M. Pohl, "Electromechanical and robot-assisted arm training for improving generic activities of daily living, arm function, and arm muscle strength after stroke," Cochrane database of systematic reviews, no. 6, 2012.

[11] H. Rodgers, H. Bosomworth, H. I. Krebs, F. van Wijck, D. Howel, N. Wilson, L. Aird, N. Alvarado, S. Andole, D. L. Cohen, et al., "Robot assisted training for the upper limb after stroke (ratuls): a multicentre randomised controlled trial," The Lancet, vol. 394, no. 10192, pp. 51–62, 2019.

[12] L. Petrich, J. Jin, M. Dehghan, and M. Jagersand, "A quantitative analysis of activities of daily living: Insights into improving functional independence with assistive robotics," in 2022 International Conference on Robotics and Automation (ICRA), pp. 6999–7006, IEEE, 2022.

[13] R. Shadmehr and F. A. Mussa-Ivaldi, "Adaptive representation of dynamics during learning of a motor task," Journal of neuroscience, vol. 14, no. 5, pp. 3208–3224, 1994.

[14] M. Desmurget and C. Prablanc, "Postural control of three-dimensional prehension movements," Journal of neurophysiology, vol. 77, no. 1, pp. 452–464, 1997.

[15] W. Abend, E. Bizzi, and P. Morasso, "Human arm trajectory formation.," Brain : a Journal of Neurology, vol. 105, pp. 331–348, 6 1982.

[16] P. Morasso, "Spatial control of arm movements," Experimental Brain Research, vol. 42, pp. 223–227, 4 1981.

[17] E. Bizzi, N. Accornero, W. Chapple, and N. Hogan, "Posture control and trajectory formation during arm movement," Journal of Neuroscience, vol. 4, pp. 2738–2744, 11 1984.

[18] B. Rohrer, S. Fasoli, H. I. Krebs, B. Volpe, W. R. rontera, J. Stein, and N. Hogan, "Submovements grow larger, fewer, and more blended during stroke recovery," Motor Control, vol. 8, pp. 472–483, 10 2004.

[19] M. Guidali, A. Duschau-Wicke, S. Broggi, V. Klamroth-Marganska, T. Nef, and R. Riener, "A robotic system to train activities of daily living in a virtual environment," Medical & biological engineering & computing, vol. 49, pp. 1213–1223, 2011.

[20] U. Keller, G. Rauter, and R. Riener, "Assist-as-needed path control for the pascal rehabilitation robot," in 2013 IEEE 13th international conference on rehabilitation robotics (ICORR), pp. 1–7, IEEE, 2013.

[21] H. J. Asl, M. Yamashita, T. Narikiyo, and M. Kawan- ishi, "Field-based assist-as-needed control schemes for rehabilitation robots," IEEE/ASME Transactions on Mechatronics, vol. 25, no. 4, pp. 2100–2111, 2020.

[22] Buccelli, Stefano, et al. "A gravity-compensated upper-limb exoskeleton for functional rehabilitation of the shoulder complex." Applied Sciences 12.7 (2022): 3364.

[23] Salthouse, Timothy A. "Adult age and the speed-accuracy trade-off." Ergonomics 22.7 (1979): 811-821.

[24] Schmidt, Richard A., et al. "Speed-accuracy trade-offs in motor behavior: Theories of impulse variability." Motor behavior: Programming, control, and acquisition (1985): 79-123.

[25] Wu, Chia-Chien, Oh-Sang Kwon, and Eileen Kowler. "Fitts's Law and speed/accuracy trade-offs during sequences of saccades: Implications for strategies of saccadic planning." Vision research 50.21 (2010): 2142-2157.

[26] Flash, T., Hogan, N. (1985). The coordination of arm movements: an experimentally confirmed mathematical model. Journal of neuroscience, 5(7), 1688-1703.

[27] Shadmehr, Reza, and Ferdinando A. Mussa-Ivaldi. "Adaptive representation of dynamics during learning of a motor task." Journal of neuroscience 14.5 (1994): 3208-3224.

[28] Kawato, Mitsuo. "Internal models for motor control and trajectory planning." Current opinion in neurobiology 9.6 (1999): 718-727.

[29] Poggio, Tomaso, and Federico Girosi. "Networks for approximation and learning." Proceedings of the IEEE 78.9 (1990): 1481-1497.

[30] A. K. Abdel-Malek, A. M. Ahmed, S. A. E. A. El Sharkawi, N. A. E. M. Abd El, et al., "Predic- tion of stature from hand measurements," Forensic science international, vol. 46, no. 3, pp. 181–187, 1990.

[31] G. Bruni, A. Bucchieri, F. Tessari, N. Boccardo, A. Marinelli, E. De Momi, M. Laffranchi, and L. De Michieli, "A multi-body model of an upper-limb prosthesis for grip force estimation and related object interaction application," in 2022 9th IEEE RAS/EMBS International Conference for Biomedical Robotics and Biomechatronics (BioRob), pp. 01–07, IEEE, 2022.